PHYSICAL REVIEW A VOLUME 24, NUMBER 3 SEPTEMBER 1981

Usefulness of x-ray diagnostics in dense-plasma gradients

D. Duston, J. Davis, and P. C. Kepple
Plasma Radiation Group, Plasma Physics Division, Naval Research Laboratory, Washington, D.C. 20375
(Received 31 March 1981)

The effect of electron temperature and ion density gradients on x-ray diagnostics for dense plasmas is studied. Time-independent calculations of the K-shell radiation spectrum from imploding wire arrays and laser-foil interaction experiments are performed using a one-dimensional collisional-radiative equilibrium ionization model with probability-of-escape radiation transport. The resulting spectra are analyzed using diagnostic techniques based on the assumption that the plasma is an isodense, isothermal emitter. It is shown that temperature determinations via line ratios and bound-free continuum slopes are affected by plasma opacity, the temperature dependence of line and continuum emission power, and the spatial ion density distribution in the plasma. Significant differences between actual and predicted values of plasma parameters are found, and the physical reasons for the discrepancies are discussed in detail.

I. INTRODUCTION

Spectroscopic analysis of radiation emission has been shown to be a powerful tool in determining plasma properties in both laboratory and astrophysical phenomena. Because of its characteristic atomic structure, a hot plasma emits a spectrum which contains a wealth of information regarding such parameters as plasma temperature, size, density, and ionization state. With the advent of high-powered lasers and pulsed-power devices came the opportunity to create and study dense plasmas in which materials were ionized to highly charged states due to the high plasma temperatures attained. Early attempts to analyze experimental spectra were usually limited to the construction of models of the ionization and radiation which concentrated on a small portion of the spectrum containing a few emission lines or a single free-bound continuum. In this way, analytic expressions for the plasma parameters were sought which did not depend on knowledge of the atomic state population densities, since determination of these quantities involved a comprehensive treatment of the plasma material's atomic structure. In low-density plasmas, such as magnetic confinement fusion plasmas and many astrophysical phenomena, the application of spectral diagnostics is facilitated by the reduced influence of particle collisions and photon reabsorption, limiting the complexity of the radiation modeling needed for accurate analyses. In higher-density plasmas such as the plasma focus, laser-produced plasmas, Z pinches, imploding wire arrays and inertial confinement fusion targets, opacity effects, particle collisions, and line broadening add new complexities to the problem of plasma diagnostics via spectral analysis, and more complex models are necessary.

In the course of spectra analysis of dense plasmas, many approximations are often invoked which enable the spectroscopist to simplify the formidable modeling task. Often, the plasma is treated as a time-independent medium, frozen in space and time during the spectral formation under the assumption that the radiation pulse is short compared to the time scale of hydrodynamic changes. Plasmas at very high densities are often treated as if they were in local thermodynamic equilibrium (LTE),[1] which allows for the application of the Saha equation and Boltzmann statistics to predict state population densities. Spectral features are also sought which result from transitions to levels of low concentration in order to minimize the effect of reabsorption of radiation due to plasma opacity[2] in analyzing these features. In some studies where opacity effects cannot be avoided, escape factors[3,4] are used to attenuate line radiation but no self-consistent account of the effect of the photon pumping on the excited levels is included.

One of the most common approximations made in spectral analysis, however, is the assumption that over some spatial region, the plasma can be characterized as an isothermal, isodense radiator. This does not imply that the plasma does not have temperature and density gradients during the emission phase, but rather, in spite of these gradients, a physically meaningful "average temperature and density" can be determined from the spectral emission from the region containing the gradients. In some laboratory plasmas (for example, the compressed core of a laser-imploded glass microballoon), the spatial temperature and density profiles may not vary significantly at the time of peak compression, and the "isodense, isothermal" assumption may be a valid approximation. In this article, we describe a unique study undertaken to assess the validity of this approximation; a radiation-ionization model is used as

the source of both experimental spectra and the theoretical analysis. We concentrate on two plasma diagnostics widely used in plasma spectroscopy: line intensity ratios and the slope of the free-bound continuum. (At the densities of interest here, Stark broadening of the observable K-shell lines is too small to be a viable density diagnostic.) We calculate the spectral emission from hypothetical aluminum plasmas with temperature and/or density gradients (as predicted by our model) and then diagnose these spectra using results calculated by our model for an isothermal, isodense plasma.

This study was born out of previous work[5-8] investigating the behavior of line intensity ratios from dense plasmas in which it was assumed that no gradients existed. From the results of this work, temperatures and densities were deduced from experimental spectra taken from imploding aluminum wire-array plasmas.[9] However, several inconsistencies were found in the data that could not be resolved with the isodense, isothermal analysis, particularly line intensities associated with satellite and intercombination lines in the K-shell spectra. Thus, our purpose here is to establish the validity of this method of spectral diagnosis or, in the case where the method is questionable, attempt to resolve the discrepancies that currently exist in the comparison of theoretical and experimental spectra.

II. THEORETICAL MODEL

The model used in this study has been reported on in detail in previous publications.[5-8] The level populations are determined by solving a set of atomic rate equations for aluminum ground states and selected excited states to obtain the fractional populations of the levels, the electron density, and the radiation emission. The system of equations is solved by setting the explicit time dependence to zero under the assumption that the plasma is in collisional-radiative equilibrium (CRE).[10] A radiation transport scheme, based on the probability of escape for line[11] and continuum[8] photons, is solved self-consistently with the rate equations in a one-dimensional multicell model to take account of radiation attentuation and photon pumping due to photon reabsorption when the plasma becomes optically thick. The atomic level structure employed in this study included all 14 ground states of aluminum plus the $n=2-10$ levels in Al XIII; the $2s\,^3S$, $2p\,^3P$, $2s\,^1S$, $2p\,^1P$, 3 triplet, 3 singlet, and $n=4-9$ levels in Al XII; the $2p$, $3s$, $3p$, $3d$, and $n=4-6$ levels in Al XI; and six doubly excited levels: $2s2p\,^3P$, $2p^2\,^3P$, $2s2p\,^1P$, $2p^2\,^1D$, $1s(2s2p\,^3P)\,^2P$, and $1s2p^2\,^2D$. All levels of an ionization stage are coupled to the ground state of the next higher ionization stage by collisional and photoionization, and by collisional, radiative, and stimulated recombination. In addition, ground states are coupled by effective dielectronic recombination. Electron collisional excitation and deexcitation couple all excited states to their respective ground state, as well as to each other, and all allowed transitions are coupled by photoexcitation and spontaneous and stimulated radiative decay. In addition, some strong dipole-forbidden transitions are also coupled by these radiative processes, such as the $1s^2$-$1s2p\,^3P$ transition. Although this is a study of K-shell ions and their characteristic radiation, inclusion of the Al XI (lithiumlike) level structure is necessary since significant population can be hidden in these levels when the plasma is near the lower end of the temperature range in which K-shell ions become dominant; this is particularly evident at higher densities. Since the Al XII ground state has a large population over a wide range of temperatures, recombination to the Al XI excited levels is not negligible, even at K-shell temperatures, and to neglect these levels in the calculation results in an incorrect ionization balance.

The methods for calculating the rate coefficients for each of these included processes are described in the earlier work. However, two changes were made in these methods which were precipitated by the extensive comparisons between theory and experiment. First, the collisional-ionization rates are now calculated by Burgess's exchange-classical–impact-parameter (ECIP) method,[12] replacing our earlier hydrogenic approximation. This resulted in an increase in the radiation from higher Rydberg levels of the K-shell in the Lyman series lines. Second, we have incorporated the recently published results of Pradhan *et al.*[13] for the electron collisional excitation rate coefficients for the transitions $1s^2$-$1s2s\,^3S$ and $1s^2$-$1s2p\,^3P$ in Al XII. This has resulted in an increase in the intensity of the $1s^2$-$1s2p\,^3P$ intercombination line of about 30% at densities of about 10^{19} ions/cm^3. This will have a large impact on the average density determination of the plasma using the intercombination and heliumlike resonance line ratio.

Our selection of the methods by which the rate coefficients are calculated is based upon the level of sophistication of the collision physics used in calculating the cross sections, as well as the significance of the effect of a cross section on the ionization balance and radiation. In some cases, hydrogenic formulas yield rates which differ only slightly from a more accurately determined value. In other instances, e.g., the electron collisional excitation rates for both direct and spin-flip tran-

sitions in Al XII and the collisional-ionization rates mentioned above, the hydrogenic formulas are unsuitable, since they give values which are in error with the results of more sophisticated methods to such an extent as to adversely affect the radiation diagnostics. While it is felt that the atomic data used in this calculation represent state-of-the-art collisional calculations, this data base is continually being updated to include the results of improved calculations, as was done with the work of Pradhan *et al.* on cross sections of critical importance to plasma-density determinations.

Since the average density of the plasmas considered in this study is 3×10^{19} ions/cm^3, no continuum lowering[1] has been included in the calculation. The lowering of the ionization potential by electron screening affects the calculation of ionization equilibrium in two ways: (1) states lying above the lowered ionization potential are pushed into the continuum and (2) ionization and recombination rate coefficients for a level below the lowered ionization limit must be calculated as a function of the new energy difference between the level and the continuum. At the average densities treated here, 3×10^{19} ions/cm^3, the lowering is small, only about 8 eV, hence the effect was not accounted for.

III. RESULTS

The study of the effect of gradients on x-ray diagnostics in a dense plasma is an enormous undertaking if one is to treat the problem comprehensively. We have therefore limited the temperature, density, and size parameters to a range corresponding to specific types of laboratory plasma; the imploding wire-array or dense-gas Z-pinch experiment, and the uncompressed region of laser-produced plasma. In addition, the investigation has been limited to x rays emitted from the K-shell ions in order to focus on lines and continua in a relatively small range of the spectra. The range of temperatures of interest for aluminum are between about 200 and 1200 eV, while the densities are typically 0.7 to 5.0×10^{19} ions/cm^3.

The K-shell x-ray emission has been chosen for investigation in view of the many earlier studies of diagnostics in this region of the spectra. In addition to the earlier work by these authors, K-shell emission has been studied in a comprehensive way by several other workers.[14-21] However, a large number of papers exist which concentrate on studying a few aspects of the K-shell emission, such as lithiumlike satellite line intensities,[22-27] intercombination lines,[28-32] heliumlike satellite lines,[5,22,25,33-35] continuum edge shifts,[36-38] Lyman α fine-structure splitting,[32,39,40] and Stark broadening of resonance series lines.[41-43] Since many of the above papers treat an isodense, isothermal plasma in applying the specific diagnostic technique of interest, the results here may have a significant effect on the conclusions drawn from previous studies.

The existence of temperature and density gradients in laboratory plasmas is a reality. The question to be addressed here is whether the gradients influence the outcome of conventional spectroscopic analysis and whether an analysis based on the isothermal, isodense assumption yields physically meaningful values for the plasma parameters. To answer this, we will generate K-shell spectra by assuming specific temperature and density profiles typical of the plasmas of interest; these will represent the "experimental" spectra. Then, these spectra will be analyzed using the techniques which have been developed from results of theoretical calculations of isodense, isothermal plasmas. The values of parameters thus obtained will then be compared to what we know to be the true parameters used in generating the radiation spectra. As was mentioned earlier, the comparisons will concentrate on line intensity ratios and continuum slopes in order to obtain values for average plasma parameters. The investigation is separated into four sections: a study of isolated linear (1) temperature and (2) density gradients (to develop some intuitive feeling for their effect on the diagnostics), (3) an analysis of an imploded aluminum wire-array plasma, and (4) an analysis of a plasma generated by laser-foil interaction. In all four cases, the temperature and density profiles have been frozen in time, presumably at the moment of peak K-shell x-ray emission. Of course, this eliminates any time-dependent behavior of the emission which may often play a role in the spectral formation. This effect can be manifested both in the modification of the temperature and density profiles as well as in the explicit time dependence of the rate equations which can cause the electron temperature to differ from the deduced ionization temperature.[22] However, our goal is to study the isolated effects of gradients on the diagnostics, while deferring the effects of time evolution to a later work.

A. Linear temperature gradient

In order to gain insight into the effect of plasma temperature and density gradients on x-ray diagnostics, a series of spectra was generated from plasmas with either an isolated temperature or density profile; in all four cases this gradient was linear with radius. The size of the K-shell emitting region was set at 250 μm (nominal size for an

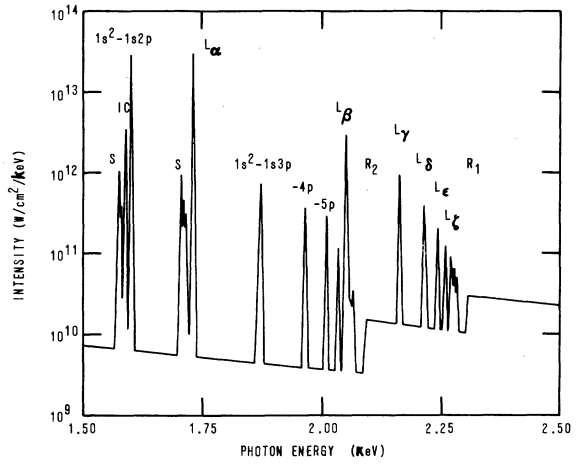

FIG. 1. Aluminum K-shell spectrum for a slab of plasma at 3×10^{19} ions/cm^3 and a 250-μm thickness. The temperature gradient is linear from 100 eV in the frontside to 1100 eV at the backside.

aluminum wire-array plasma at compression) and a slab geometry is employed to allow the gradient to be truly linear, eliminating weighting effects due to different zonal volumes.

In the first two calculations, the assumed temperature gradient ranged linearly from 100 to 1100 eV, yielding an average plasma temperature of 600 eV (again, typical of wire-array plasmas). While one may argue that this gradient is exaggerated, only trends in the diagnostics are being investigated at this point. The spectra from the two calculations are shown in Fig. 1, where the higher temperature occurs in the zone farthest from the "spectrometer" and in Fig. 2, where it occurs in the nearest zone. The ion density is

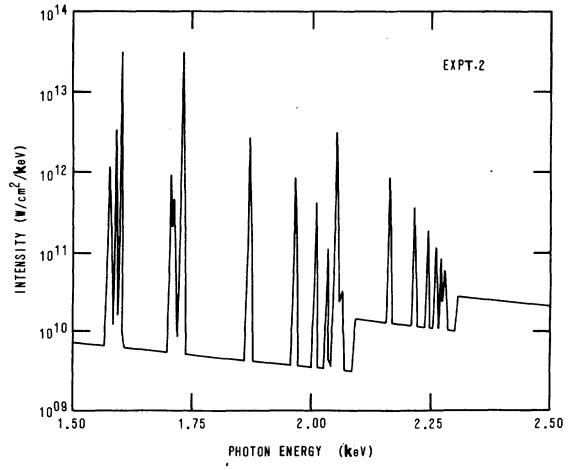

FIG. 2. Aluminum K-shell spectrum for the plasma conditions of Fig. 1, but with a linear temperature gradient from 1100 eV in the frontside to 100 eV at the backside.

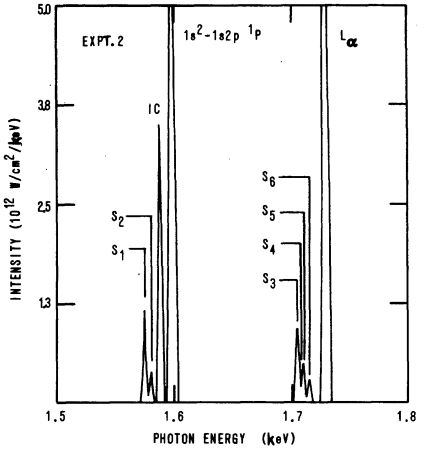

FIG. 3. Aluminum K-shell spectrum for the plasma in Fig. 2, showing the 1.5–1.8-keV range expanded.

held at a constant value of 3×10^{19} ions/cm^3 for both calculations.

The first step in diagnosing the plasma, assuming the spatial depth of 250 μm has been measured (from x-ray pinhole photographs, for example), is to determine a possible range for the average plasma density. To do this, two line ratios are used: (1) the $1s^2$-$1s2p\,^3P/1s^2$-$1s2p\,^1P$ intercombination-(IC)-to-resonance line ratio and (2) the $1s2p\,^3P$-$2p^2\,^3P/1s2s\,^3S$-$2s2p\,^3P$ line ratio; these last two lines are satellites, identified in Fig. 3 (a magnified section of Fig. 2) by S_5 and S_4, respectively. The values of these two line ratios for isothermal, isodense plasmas are shown in Fig. 4, as a function of ion density, for electron

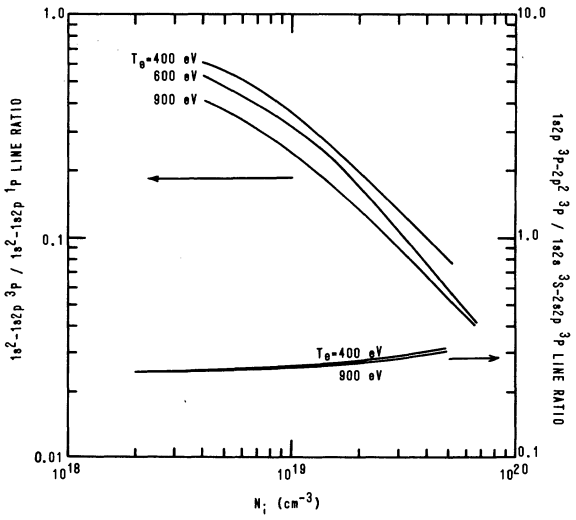

FIG. 4. Density-sensitive line intensity ratios versus ion density for 400-, 600-, and 900-eV electron temperatures (slab geometry, 250-μm-thick aluminum plasma).

TABLE I. Ion densities and electron temperatures deduced from selected emission line intensity ratios and bound-free continuum slopes for the seven calculations of plasmas with gradients. Also given are the volume-averaged densities and temperatures of the plasmas.

Expt. number	Average T_e (eV)	Average N_I (ions/cm^3)	Density diagnostics $\frac{1s^2\text{-}1s2p\,^3P\ (IC)}{1s^2\text{-}1s2p\,^1P}$	Density diagnostics $\frac{1s2p\,^3P\text{-}2p^2\,^3P}{1s2s\,^3S\text{-}2s2p\,^3P}$	Electron temperature diagnostics $\frac{1s\text{-}2p\ (L\alpha)}{1s^2\text{-}1s2p\,^1P}$	$\frac{1s\text{-}2p\ (L\alpha)}{1s^2\text{-}1s3p\,^1P}$	$\frac{1s\text{-}3p\ (L\beta)}{1s^2\text{-}1s4p\,^1P}$	$\frac{1s\text{-}3p\ (L\beta)}{1s^2\text{-}1s5p\,^1P}$	$\frac{1s\text{-}4p\ (L\gamma)}{1s^2\text{-}1s5p\,^1P}$	$\frac{1s^22p\text{-}1s2p^2\,^2D\ (j\text{-}k)}{1s^2\text{-}1s2p\,^1P}$	$\frac{1s2p\,^1P\text{-}2p^2\,^1D}{1s\text{-}2p\ (L\alpha)}$	Al XIII free-bound continuum slope	Al XII free-bound continuum slope
1	600	3 × 10^{19}	2.5 × 10^{19}	2.7 × 10^{19}	735		1100	900	925	720	765	701	527
			4.0 × 10^{19}	3.3 × 10^{19}	710		1050	900	915	730	780		
2	600	3 × 10^{19}	3 × 10^{19}	2.7 × 10^{19}	725	770	850	845	825	705	775	676	544
			4.4 × 10^{19}	3.3 × 10^{19}	705	555	860	860	820	710	785		
3	600	3 × 10^{19}	2.9 × 10^{19}	2.6 × 10^{19}	715	450	690	760	685	610	785	750	613
			4.2 × 10^{19}	3.2 × 10^{19}	690	400	700	785	690	615	790		
4	600	3 × 10^{19}	3.1 × 10^{19}	3.3 × 10^{19}	620		600	565	610	595	600	611	573
			4.4 × 10^{19}	4.2 × 10^{19}	595	700	615	585	610	590	600		
5	600	3 × 10^{19}	3.0 × 10^{19}	3.3 × 10^{19}	615	980	615	600	615	600	600	613	602
			4.4 × 10^{19}	4.2 × 10^{19}	590	565	625	615	620	590	595		
6	275	1.75 × 10^{19}	2.8 × 10^{19}	4.0 × 10^{19}	665		1020	865	845	525	680	623	477
			4.2 × 10^{19}	4.8 × 10^{19}	645		1000	870	840	525	680		
7	771	3.5 × 10^{19}	2.0 × 10^{19}	4.5 × 10^{19}	695	620	665	645	700	435	590	400	205
			5.0 × 10^{19}	6.0 × 10^{19}	500		460	485	500	625	665		

temperatures between 400 and 900 eV. Once the density range is diagnosed, several other line ratios are used to determine the average plasma temperature: (1) $L\alpha/1s^2\text{-}1s2p\,^1P$, (2) $L\alpha/1s^2\text{-}1s3p\,^1P$, (3) $L\beta/1s^2\text{-}1s4p\,^1P$, (4) $L\beta/1s^2\text{-}1s5p\,^1P$, (5) $L\gamma/1s^2\text{-}1s5p\,^1P$, (6) $1s^22p\,^2P\text{-}1s2p^2\,^2D/1s^2\text{-}1s2p\,^1P$, and (7) $1s2p\,^1P\text{-}2p^2\,^1D/L\alpha$. The $1s^22p\,^2P\text{-}1s2p\,^2D$ satellite line (j-k satellite) is labeled S_1 in Fig. 3, while the $1s2p\,^1P\text{-}2p^2\,^1D$ is indicated by

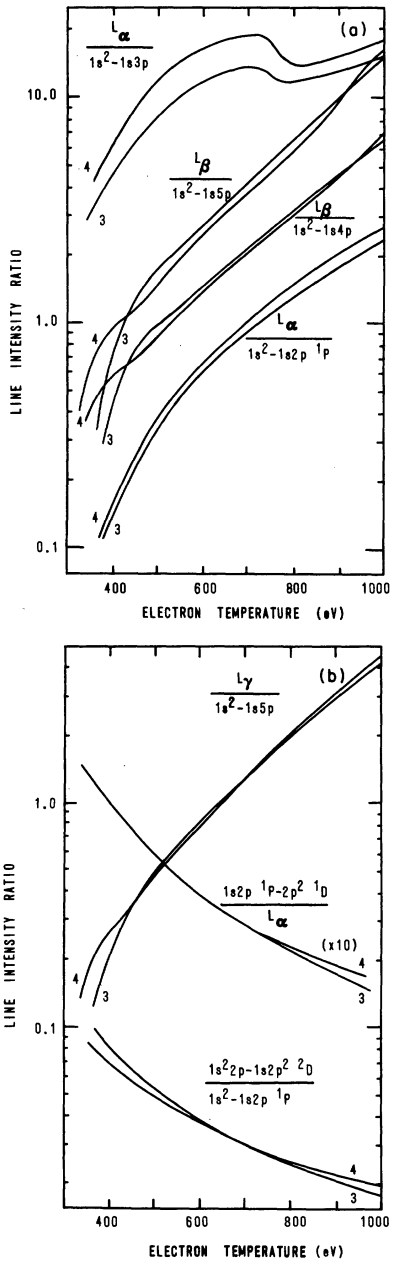

FIG. 5. Temperature-sensitive line intensity ratios versus electron temperature for aluminum plasma of 250-μm thickness at 3×10^{19} and 4×10^{19} ions/cm^3.

S_3. The remaining two satellite lines, the $1s2s\,^1S$-$2s2p\,^1P$ (S_6) and the $1s^22s\,^2S$-$1s(2s2p\,^3P)\,^2P$ (q-r satellite, S_2) transitions, are normally too weak to be used for accurate predictions. The values of these seven line ratios vs electron temperature for a 250-μm aluminum plasma at 3.0 and 4.0 $\times 10^{19}$ ions/cm^3 are shown in Fig. 5. One could conceivably generate a large number of line intensity ratios using every possible combination of a hydrogenlike and a heliumlike K line to determine a temperature. In practice, the photographic film response may not be accurately known over a wide frequency range or absorption edges of various filters may be in the spectral range of interest. Hence, it is preferable that only lines which are close lying in the spectra be used to construct line intensity ratios. Finally, the slope of the free-bound continuum is measured from the spectra and a temperature is calculated,[1] since the free-bound intensity scales as

$$I_{fb} \sim \exp[-(E - E_0)/T_e], \quad (1)$$

where E is photon energy, E_0 is the energy of the recombination edge, and T_e is electron temperature. The spectral plots in Figs. 1 and 2 have been plotted with the spectral intensity on a logarithmic scale to more clearly illustrate the free-bound continuum. Two such continuum edges exist in the K-shell spectra, the bare nucleus-to-1s and the 1s-to-1s^2 recombination edges (designated R_1 and R_2 in Fig. 1); the energy regions containing the slopes of interest extend to the high-energy side of these edges, hence two measurements of temperature are obtainable from the K spectra using this technique. Of course, the continuum also receives a contribution from bremsstrahlung (free-free) emission, but in plasmas under investigation here, the free-free continuum is negligible in the spectral range being studied.

Thus, the list of spectral diagnostics employed includes two density-sensitive line intensity ratios, seven temperature-sensitive line intensity ratios, and two temperature-sensitive free-bound continuum slopes. The results of all these diagnostics as applied to the experimental spectra are shown in Table I, where the parameters deduced from the spectra in Figs. 1 and 2 are listed as expt. 1 and expt. 2. The first interesting point to note from the tabulated data is that the range of densities deduced from the line ratios (assuming an uncertainty in temperature from 400 to 900 eV) extends from 2.5 to 4.4 $\times 10^{19}$ ions/cm^3, but centers on the actual density in both runs of 3×10^{19} ions/cm^3. Thus, the temperature gradient has not disturbed the density determination to any significant degree. The density determination from the two satellite lines is the less reliable of the two, since the ratio is somewhat insensitive at this density (see Fig. 4); however, a value for ion density can still be obtained from this diagnostic if good spectral resolution has been achieved.

In actual experimental spectra, these two satellite lines lie very closely spaced, and high spectral resolution is required to obtain an accurate ratio. For higher-Z materials, the individual j components of the lines may be blended together; this renders the ratio unusable if the lines are significantly broadened, even with high spectral resolution. With appropriate frequency-by-frequency radiation transport calculations, however, the *manifold* of the two transitions can be compared to, say, the $1s2p\,^1P$-$2p^2\,^1D$ satellite transition to form an appropriate density-sensitive line intensity ratio. In the case of aluminum, the plasma density should exceed about 10^{20} ions/cm^3 before this ratio can be used accurately. In addition, whenever satellite lines are used for diagnostics in very high-density (e.g., laser-compressed pellet) plasmas, some account should be taken of the Stark broadening. To our knowledge, no self-consistent calculation of the Stark broadening of overlapping emission lines *from autoionizing levels* exists, although Jacobs and Davis in their study of isolated lines,[44] suggest that to first order the widths are scalarly additive. A study of this problem as it relates to high-density plasma diagnostics is currently underway.

Since the density determination yielded a small spread in values, the temperatures deduced from the seven line ratios were obtained for two values of density, 3 and 4×10^{19} ions/cm^3, as shown in Table I. In spite of this density spread, the temperatures determined from all seven line ratios show only small differences due to the density uncertainty, but all are higher than the 600-eV average temperature of the plasmas in experiments 1 and 2, except for the $L\alpha/1s^2$-$1s3p$ ratio. In the first case, this ratio is so large that no temperature prediction could be made (see Fig. 5), while in the second case, the temperature uncertainty is over 200 eV, very substantial compared to the 10–20-eV differences obtained from the other ratios over the possible range of densities. From Fig. 5 it can be seen that opacity alone has an adverse effect on this line intensity ratio, since it becomes double valued at higher densities. The added effects of the temperature gradients drive this ratio to higher values than can be found on the curves; clearly, this line ratio is very inaccurate in the regime of temperatures and densities of interest here, and hence, will be ignored in all following discussions.

In addition to the fact that all of the remaining six line ratios yield temperatures which universal-

ly lie above the average plasma temperature, the values vary over such a wide range (705–1100 eV) that no conclusive statement can be made about the average plasma temperature from these results. Even if one were to average the temperatures deduced from these line ratios, the values obtained for the two plasmas (853 and 789) are still quite far from the actual average temperature of 600 eV. In view of this result, two important phenomena are evident and warrant detailed discussion: (1) the direction of the temperature gradient affects the diagnosis of the plasma temperature and (2) the diagnosis yields higher average temperatures than the actual average temperature regardless of the direction of the gradient.

The difference of about 60 eV due to the direction of the temperature gradient is easily understood from opacity effects alone. For a radiating plasma in slab geometry, the frontside emission reaches the spectrometer only slightly affected by opacity because of the small path length traversed by the photons. Radiation from the backside, however, must pass through the entire plasma before exiting on its way to the spectrometer and is strongly reabsorbed (depending on the density and thickness) along its path length. Since the temperature gradient assumed here spans the range typical of both hydrogenlike and heliumlike line emission, the direction of the gradient affects the diagnostics. Photons emitted in the backside and reabsorbed in the frontside "optically pump" the excited levels in the front zones from which ionization to a higher ion now proceeds at a faster rate. The net effect is an ionization temperature in the frontside which exceeds the electron temperature there. This will raise the value of the "average temperature" somewhat, regardless of the direction of the temperature gradient. In order to substantiate this, expt. 3 was run for plasma conditions identical to expt. 1 but in an "optically thin" approximation; the results are shown in Table I. The average plasma temperature from this calculation (from line ratios) was 710 eV, higher than the actual 600-eV average (since it was optically thin, the direction of the gradient had no effect on the emission), but lower than the average temperatures of experiments 1 and 2. Thus, opacity raises the average ionization temperature of the plasma somewhat above the average electron temperature. However, the degree to which it is raised depends on the *direction* of the temperature gradient. If we look at the temperature values predicted by individual line ratios for experiments 1 and 2 in Table I, the $L\alpha/1s^2$-$1s2p$, $1s^22p$-$1s2p^2/1s^2$-$1s2p$, and $1s2p\,{}^1P$-$2p^2\,{}^1D/L\alpha$ line intensity ratios exhibit only minor differences due to the gradient's direction. However, the $L\beta/1s^2$-$1s4p$, $L\beta/1s^2$-$1s5p$, and $L\gamma/1s^2$-$1s5p$ line ratios, all involving higher Rydberg members of the K-shell ions, yield significantly higher temperatures for the gradient with a hotter backside and cooler frontside than for the reverse gradient. In the former plasma, mainly hydrogenlike line photons from the backside pass through cooler zones on the frontside, exciting the Al XIII ground-state ions found at that cooler temperature; the pumped Al XIII excited states ionize more rapidly to the bare nucleus where recombination again occurs, with the net effect of enhancing Al XIII line emission. On the other hand, when heliumlike line photons must pass through hotter plasma regions, as in the case of the cooler backside-hotter frontside plasma, a large population of Al XII ground states still exists in the hotter zones (for a discussion of the persistence of closed-shell ionic systems over wide temperature ranges, see Ref. 6), resulting in *significant* pumping of the Al XII excited levels in the hot frontside, and an enhancement of the heliumlike lines. The preferential intensification of these Al XII lines for the plasma temperature gradient in expt. 2 will yield a *lower* temperature from the line ratios comprised of a hydrogenlike and heliumlike emission line, since the heliumlike line appears in the denominator of these line ratios. The value of the line ratio will be decreased by the enhanced heliumlike line, lowering the predicted temperature as compared to a plasma, as in expt. 1, where the gradient is reversed and hydrogenlike lines are enhanced. Thus, the 60-eV average temperature difference between experiments 1 and 2 is explained by line reabsorption and radiation transport.

The second phenomenon to be explained is the higher average temperature predicted by these line ratios as compared to the actual average temperature, irrespective of the gradient direction. It was found in the discussion above, that an optically thin calculation (expt. 3) containing identical plasma conditions to expt. 1, yields an average temperature of only 710 eV, and that the increase from 710 to 850 eV in expt. 1 and from 710 to 790 in expt. 2 was due to opacity effects. Hence, a large fraction of the temperature increase over the actual average 600-eV temperature of the plasma must be due solely to collisional effects within a gradient environment. To substantiate this hypothesis, a calculation was done for an optically thin isothermal plasma at 600 eV (other conditions were the same as expt. 3) and the results compared with expt. 3. The line ratios comprised of hydrogenlike and heliumlike lines were consistently larger for the plasma with the temperature gradient. The explanation of this effect is based on the fact that the K-shell line emission peaks at

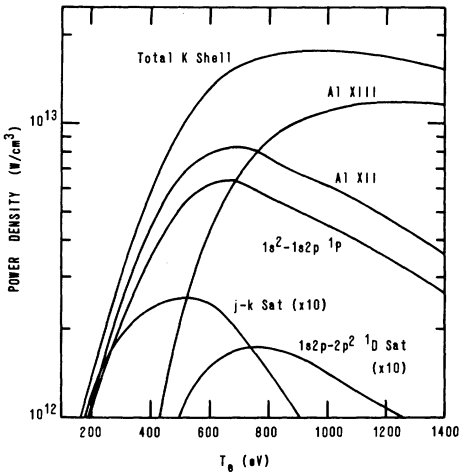

FIG. 6. Al XII, Al XIII, $1s^2$-$1s2p$, j-k satellite, $1s2p$-$2p^2\,{}^1D$, and total K-shell line emission power density versus electron temperature for an isothermal cylindrical plasma with radius of 250 μm and a density of 3×10^{19} ions/cm^3.

temperatures near the highest value of temperature in our assumed gradients. This is shown in Fig. 6, where the Al XII and Al XIII line emission power density is plotted as a function of electron temperature for an isothermal 250-μm radius cylindrical plasma at 3×10^{19} ions/cm^3. Hence, line emission from the K shell is more intense from the hotter end of our gradient than from the cooler end. In the line ratio diagnostics, this will be manifested as an effective weighting of the line ratio, preferentially toward the *hot* end of the gradient where more power is being radiated. Hence, for a plasma in this temperature regime (even an optically thin one) in which a temperature gradient exists, certain line ratios will predict higher temperatures than the *actual* average plasma temperatures.

At this point, a brief discussion of the satellite line emission, as it pertains to temperature gradients, is required. Satellites to the long-wavelength side of the heliumlike resonance line have been the subject of many studies,[22-27,45-48] several of which noted some discrepancies between theoretically predicted values and experimentally measured spectra. Many explanations for disagreement have been suggested, e.g., time-dependent behavior of the emission, a Z scaling of the atomic parameters, errors in atomic data determinations, rate coefficients, or abundance curves, etc. It can be shown from this study, that the cooperative effects of opacity and gradients in temperature will generate emission for the j-k satellite line which will be interpreted as indicating significantly different plasma temperatures than other diagnostics. The problem of anomalous temperature predictions from the $1s^22p$-$1s2p^2/1s^2$-$1s2p$ line ratio confounded many of our earlier attempts to diagnose experimental spectra. The cause of the misinterpretation is due to both effects discussed earlier. Essentially, the two lines comprising the ratio are from levels which are both populated from the Al XII ground state. One basic difference, however, is that the $2p$ level is pumped by photons absorbed by the $1s^2$ state, whereas the $1s2p^2$ is pumped by photons from the $1s^22p\,{}^2P$ level, which is of low concentration for temperatures at which the K-shell ions are abundant. The gradient effects alone do not affect the ratio since the power densities of both lines peak at about 500–650 eV for the plasma conditions of interest (see Fig. 6). This is also substantiated by comparisons of optically thin runs with (expt. 3) and without a gradient; little difference was found in the value of this line ratio. In addition, opacity effects, alone, cause little change in the line ratio, since collisional quenching of the resonance line photons is weak at the density and size of plasmas being currently studied and the plasma is effectively thin for this line. The two effects *together*, however, cause the preferential pumping of the $1s2p\,{}^1P$ level, a reduction in the value of the line ratio, and a predicted temperature higher than the actual average plasma temperature, as can be seen in Table I, experiments 1 and 2. However, due to the different temperature scaling of the power densities of the Al XIII and $1s^22p$-$1s2p^2$ lines, this predicted temperature is always equal to or less than the predicted temperatures obtained from the other line ratios, as is also seen in Table I. Hence, in the analysis of several temperature diagnostics in the K shell using an isothermal plasma theory, the j-k satellite-to-resonance line ratio may often predict *lower* plasma temperatures, inconsistent with other diagnostics. Notice this is not the case with the line ratio formed by the $1s2p\,{}^1P$-$2p^2\,{}^1D$ satellite and $L\alpha$ lines, since this satellite's power density peaks at about 800 eV (like the Al XII line emission in Fig. 6), the ratio is strongly affected by the temperature gradient (see Table I, expt. 3), and behaves similarly to the other line ratios comprised of a hydrogenlike and heliumlike line.

Unlike the line intensity ratios, the slopes of the two free-bound continua in Figs. 1 and 2 yield temperatures which are close to the actual average temperature as seen in Table I. In fact, if one averages the results obtained for the Al XII and Al XIII continuum emission, the values obtained (614 and 610 eV for experiments 1 and 2) are very plausible estimates of the actual average temperature. Of course, the bare nucleus-to-1s recombination radiation yields a higher temperature than the

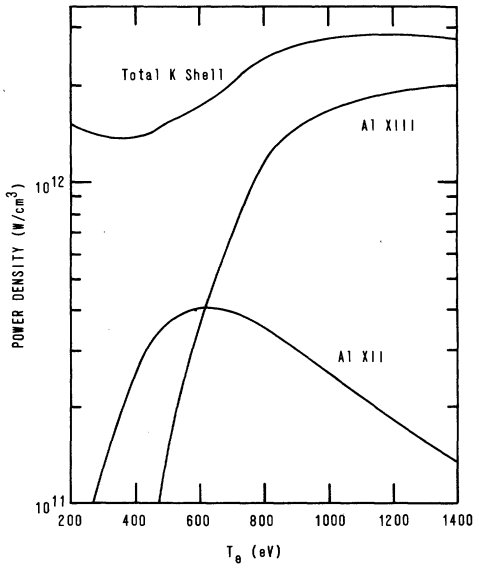

FIG. 7. Bare nucleus-to-1s and 1s-to-1s^2 radiative recombination continua power densities versus electron temperature for identical plasma conditions as in Fig. 6; the total bound-free continuum power is also shown.

1s-to-1s^2 emission since the bare nuclei will occur in higher proportion in hotter regions of the plasma, while ions in the 1s level will be found mainly in relatively cooler zones. The explanation for why the bound-free continuum slope measurements yield values for T_e close to the average value is solely dependent on the power-density variation with temperature (shown in Fig. 7). The optical depths at the frequency edge for the two recombination continua studied here are less than 0.1 in the plasma of interest, thus opacity plays little role in the temperature determination for these plasmas. From Fig. 7 it is apparent that the bare nucleus-to-1s continuum will be slightly weighted to higher temperatures since the peak occurs at about 1400 eV; the 1s-to-1s^2 continuum, on the other hand, peaks at about 600 eV, and will be slightly weighted in favor of lower temperatures due to this power-density distribution. Since the temperature gradients considered here range from 100 to 1100 eV, the bare nucleus-to-1s continuum power density exhibits a much steeper rise within this range than the 1s-to-1s^2 continuum; hence, one expects the former continuum slope to yield a result for T_e which is farther from the 600-eV average than the latter, which has a power density which changes relatively little over the same range. The results in Table I confirm this observation.

B. Linear density gradient

Studies of a sample density gradient result in a much different series of observations than the temperature gradient runs. In experiments 4 and 5, an ion density gradient was assumed which ranged linearly with radius from 1 and 5×10^{19} ions/cm^3; in expt. 4 the frontside of the slab was the lower-density surface, while the gradient was reversed for expt. 5. From Table I, it is seen that the density gradient has very little effect on any of the temperature diagnostics, either line intensity ratios or continuum slopes (with the exception of the $L\alpha/1s^2$-1$s3p$ line ratio which, once again, displays very anomalous results). The two density determinations yield values from 3.0 to 4.4×10^{19} ions/cm^3 which is slightly higher than the mean- or volumed-averaged density. If the density is averaged over ion number, however, reflecting the fact that there are more emitters in the denser regions, the average value is 3.44×10^{19} ions/cm^3. In fact, the value predicted by the line ratios for ion-density determinations will usually be weighted toward high density, since the line emission scales approximately as N^2 at these (nearly coronal) densities. This scaling reduces to linear in N as the density is increased to higher values,[7] so the weighting due to power-density scaling with N will probably have a decreasing effect on the line ratio determinations in higher density regimes than treated here. In this study of density gradients, therefore, the results have little or no effect on most of the plasma diagnostics of interest here. It must be stated, however, that a density gradient will probably have a significant effect on the diagnostics when, unlike the previous cases, a temperature gradient also exists in the plasma. The next two sections deal with such a situation *vis à vis* simulated laboratory-plasma environments.

C. Imploding wire-array plasma

In this section, the radiation from a plasma created by driving a large current through an array of aluminum wires is studied.[49] After the current vaporizes and ionizes the wires, the magnetic fields drive the plasma inward until it assembles on axis, creating a hot, dense cylindrical plasma, strong in aluminum K-shell emission.[50] This emission pulse is short compared to the time scale on which hydrodynamic changes occur, so by taking a density and temperature profile from magneto-hydrodynamic (MHD) code calculations[51] which typify plasma conditions during this short pulse, the CRE ionization-radiation model can be used to calculate a spectrum similar to an experimentally measured one. The profiles used in this calculation are shown in Fig. 8, while the resulting spectrum is shown in Fig. 9; the spectral intensity has been plotted on a linear scale to illustrate the appearance of an actual experimental spectrum.

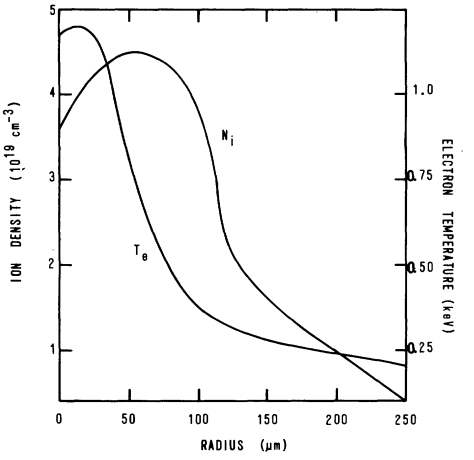

FIG. 8. Electron temperature and ion density as a function of cylinder radius for an aluminum imploding wire-array plasma. The K-shell emitting region is typically 250 μm at the time of peak radiation power (MHD calculation).

The spectrum in Fig. 9 is split into two sections (between the $L\alpha$ and the $1s^2$-$1s3p$ lines) with the higher-energy section magnified ten times. In this way the ratios of the higher Rydberg lines can be seen more easily, corresponding to the case where a spectroscopist allows stronger lines to saturate his film (usually in the first order of the crystal), thereby enhancing the appearance of the weaker lines and facilitating measurement of them. The results of various line ratios and continuum slope measurements are given in Table I under expt. 6; the volume-average temperature 275 eV, and density 1.78×10^{19} ions/cm^3, are also given. (Volume average in the sense used here and in the future implies unit length in the case of a cylindrical

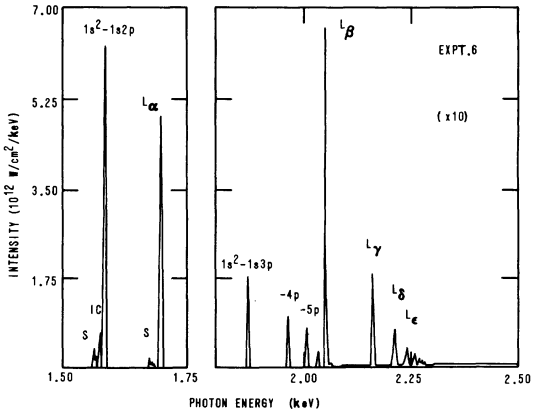

FIG. 9. Aluminum K-shell spectrum for an imploded wire-array plasma. The temperature and density profiles used in the CRE model calculation are shown in Fig. 8.

plasma and unit area in the case of a planar plasma; this is a natural consequence of the one-dimensional model. Spectral intensities are always given as power per unit surface area or power per unit volume of plasma.) The values for the $L\alpha$/$1s^2$-$1s3p$ ratio are again not usable since they yield a ratio which falls above any of the curves in the density range indicated by the density diagnostics, and will be ignored.

The density-sensitive line ratios yield a value for the density between 2.8 and 4.8 ions/cm^3. This is significantly higher than the average density of 1.75×10^{19} ions/cm^3. From the earlier studies of temperature gradients, this difference can be attributed partly to the weighting of the line emission by the line power functions. Since both lines comprising the intercombination-to-resonance line ratio are AlXII lines, they radiate strongest from 600–700 eV (see Fig. 6), thus the value of the line ratio at this temperature will be strongly weighted over other cooler and hotter regions. From Fig. 8, the plasma density is about 4.5×10^{19} ions/cm^3 in the region where the temperature varies from 600 to 700 eV; hence, the density predicted by the ratio will be biased toward this density on account of this behavior of the line power functions with temperature. In addition, it is clear that a line (or a continuum edge) will radiate with more power in high-density regions than in low-density regions. This effect adds an additional weighting to both density and temperature diagnostics in the high-density zones of Fig. 8, i.e., from the cylinder axis to about 100 μm, where the temperature averages about 800 eV and the density averages about 4×10^{19} ions/cm^3. In cylindrical geometry, the outer regions of the plasma are more heavily weighted due to volume, so the lower density in these regions will counteract this power-function and high-density weighting somewhat. However, its obvious that the value for this line ratio is heavily influenced by effects not considered in an isothermal analysis.

The range of densities determined above were used to define the conditions for generating the line ratio values for the temperature diagnostics. The two sets of temperature values given in Table I for expt. 6 are obtained for cylindrical, 250-μm radius plasmas at 3×10^{19} and 4×10^{19} ions/cm^3, approximately the range indicated by the IC-to-resonance line ratio. Note that the spread of temperatures as defined by the density range is less than 20 eV. The average temperature obtained from the six temperature-sensitive ratios is 763 eV, well above the volume-averaged temperature of 275 eV and the ion-averaged temperature of 408 eV. The three line ratios comprised of the higher Rydberg lines yield higher temperatures

than the ratios involving the satellite lines or the ratio of the resonance lines, as was the case in experiments 1 and 2. The difference between the actual and calculated average temperatures is much greater in this run, however. The reason, of course, is the density effect on the emission, as discussed above for the intercombination-to-resonance line. In addition to the high-temperature weighting due to the power function, the increased number of emitters in high-density regions biases the emission in those zones. In the case of this wire plasma, the dense zones are also the regions of high temperature, causing the diagnosis to be even *more* weighted toward the larger temperatures. This effect is evident in the temperature determinations from the continua also; both continua indicate temperatures higher than the average, due to the density and power-function weighting. Opacity of the plasma, no doubt, plays a role in the high temperatures calculated, since the temperature gradient is similar to that in expt. 1: a hot inner region with a colder surface nearer to the spectrometer. Note once again, however, that the existence of a colder region of plasma is indicated by the ratio of the j-k satellite-to-resonance line. Significant differences between the temperature deduced from this diagnostic and that deduced from the other line ratios is apparently a spectral indicator of temperature gradients.

D. Laser-produced plasma

The final investigation of plasma gradients involves the interaction of an intense laser beam with an aluminum foil target. At high laser energies, these experiments yield information about target ablation and acceleration[52] and, therefore, are important in the area of laser-fusion studies. At lower laser energies, the blow-off region between the laser and the slab target is rich in intense spectral lines and, therefore, is of interest to spectroscopists for both line classification and plasma diagnostic development. Previous theoretical calculations of laser-slab interaction[53] have shown the blow-off plasma to be essentially a two-dimensional phenomena, similar to an azimuthally symmetric plume. Thus, the radiation spectrum will differ depending on the position of the spectrometer. A one-dimensional hydrodynamic calculation,[54] which assumes a slab geometry, was employed to generate density and temperature profiles versus thickness l for the CRE calculation; hence, the radiation emission was modeled similarly, with no account taken fo the x-y (plane of the foil) dependence of plasma parameters. The spectrum calculated, therefore, is approximately what would be detected from a spectrometer placed

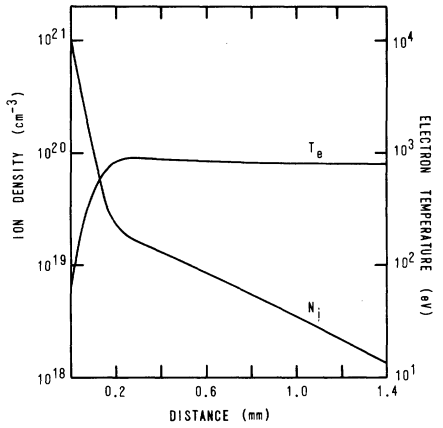

FIG. 10. Electron temperature and ion density as a function of blow-off distance for a laser-produced plasma at the time of maximum emission power. The interaction is between frequency-doubled neodymium-glass laser light (10^{13} W/cm^2, 3-nsec FWHM) and a 4-μm aluminum foil target (hydrodynamic calculation).

directly in front of (facing) the slab, with the plasma blow off in the direction of the detector. The hydrodynamic calculation modeled the interaction of a 3-nsec [full width at half maximum (FWHM)], frequency-doubled (0.53-μm) neodymium-glass laser pulse (intensity of 10^{13} W/cm^2) with a 4-μm-thick aluminum slab. The density and temperature profiles used in the CRE calculation, shown in Fig. 10, correspond to the time of peak K-shell emission, approximately 10 nsec after the peak of the laser pulse. The $l = 0$ point in the figure corresponds to the position of the front surface of the foil before laser heating is initiated. The result-

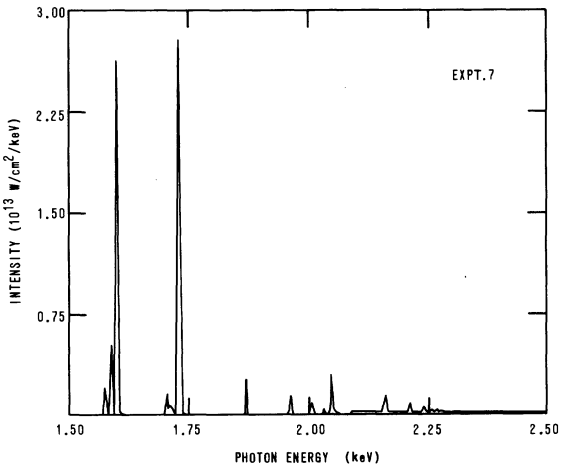

FIG. 11. Aluminum K-shell spectrum from the blow-off region of a laser plasma. The temperature and density profiles used in the CRE model calculation are shown in Fig. 10.

ing K spectrum is shown in Fig. 11 and the parameters deduced from the various diagnostics are found in Table I under expt. 7.

The temperature and density profiles in Fig. 10 are very different from those of the wire array plasma in Fig. 8 since, in the laser shot, the dense-plasma region is cold while the more rarefied plasma is hot. We saw that the power-function and -density weighting of the emission were cooperative effects in the wire plasma because of the coincidence of both hot and dense regions in the plasma. This is not the case for the laser-foil interaction. Hence, the power-density function should weight the diagnostics in the hotter, outer zones of the blow off, while the high density weights the diagnostics in the colder inner zones, near the original foil surface. Opacity effects will optically pump the plasma to a higher ionization state but may *preferentially* pump either Al XII or Al XIII excited states, so its effect on the diagnostics is strongly dependent on the magnitude of the other effects. An immediate indication as to which of these effects will dominate is given by the zonal emission intensities, i.e., the radiation intensity that reaches the spectrometer from each cell, as shown in Fig. 12 for the $1s^2$-$1s2p\ ^1P$, $1s^2$-$1s2p\ ^3P$, $1s$-$2p$, $1s^2$-$1s3p$, $1s$-$3p$, and $1s^22p$-$1s2p^2\ ^2D$ lines. This type of plot is extremely valuable, since one can determine at a glance, from which plasma regions the radiation is emanating. A brief discussion of this graph will follow in order to illuminate the later analysis of the results in Table I.

The most obvious feature of all six line intensities in Fig. 12 is the peak intensity occurring at

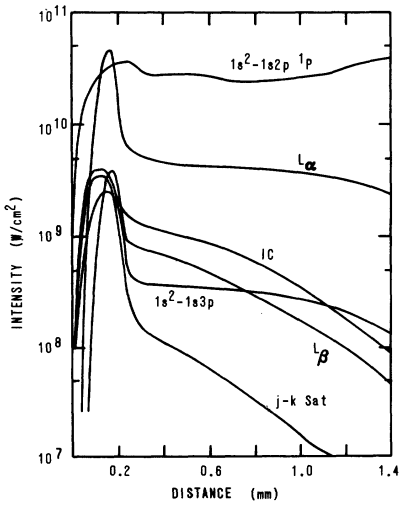

FIG. 12. Spatial contribution to the emission intensities of selected K-shell lines versus position in the plasma blow off for a laser-foil interaction experiment. The plasma conditions are identical to those given in Fig. 10.

about 0.015 cm from the original target surface. Since the lines are all from K-shell ions, the temperature interior to this point is below the "turn-on" temperature, so no significant emission occurs in spite of the high density. Exterior to this point, the density falls off rapidly while the temperature is maintained at a relatively constant level; thus, one would expect the line intensities to fall off in a similar way. This is, in fact, the case for the intercombination and j-k satellite lines; their line-center optical depths (τ_0) are on the order of 0.1, measured from the intensity peak outward, and opacity affects them only slightly. The intercombination line falls off less rapidly with radius, since the lower the density drops, the smaller is the collisional quenching of the line due to electron collisions from the $1s2p\ ^3P$ level to other $n=2$ states. The $L\beta$ and $1s^2$-$1s3p$ lines show clear peaks and fall offs similar to the intercombination line, although their line-center optical depths are about 5 and 7, respectively, from the peak emission point outward. The two resonance lines, however, show distinctly different behavior. The large peak is slightly less obvious for the $L\alpha$ line ($\tau_0=33$) and it is extremely opacity attenuated for the $1s^2$-$1s2p$ line ($\tau_0=43$) so that it appears as only a weak hump on the intensity function. Also striking is the effect of optical pumping from the resonance line ($L\alpha$) photons, which sustains the level of the emission of that line (after the initial drop with density) at a fairly constant level out to the leading edge of the blow off. However, the $1s^2$-$1s2p$ emission actually increases a bit with radius since the large optical depth has made it somewhat of a "surface emitter." As concerns the diagnostics, however, it is apparent that the emission from the various lines reflects conditions in different (or all) regions of the plasma.

From Table I, expt. 7, the density has been determined to be in the range of $(2.0\text{–}6.0)\times10^{19}$ ions/cm^3. This is a wider range of uncertainty than in the wire plasmas, but understandable in view of the fact that the actual density is more widely varying in the laser shot. The actual volume-averaged density is 3.5×10^{19} ions/cm^3, so the estimate is centered about the average. The temperature-sensitive line ratios were calculated for an isodense, isothermal plasma in this geometry for this thickness (0.14 cm) and used to determine the electron temperature values for each line ratio. The two values given for each ratio correspond to 2.0 and 5.0×10^{19} ions/cm^3 in Table I. Neglecting the $L\alpha/1s^2$-$1s3p$ line ratio, the average temperature obtained from the remaining six ratios is 580 eV, lower than the actual volume-averaged temperature of 771 by 200 eV. The difference is not nearly as striking as it was for the wire experiment, how-

ever, since the density- and power-function weighting of the emission are now *competing* effects. One significant difference from the previous results is the much wider range of diagnosed temperatures due to the uncertainty in density. This is partially due to the wider range of densities, but most of it can be accounted for by the larger size of the plasma. At a thickness of 0.14 cm, the opacity effects are such that the slopes of the line ratio functions versus T_e for an isothermal, isodense plasma are much less steep than are shown in Fig. 5 for a 250-μm-thick plasma. Consequently, there are greater uncertainties in temperature for a given density range in the thicker plasma than for the thinner one. For the laser shot, these differences are about 200 eV from 2.0 to 5.0×10^{19} ions/cm^3, except for the $1s2p$-$2p^2\,{}^1D/L\alpha$ ratio, which remains relatively density insensitive. The four ratios not comprised of a satellite line yield lower temperatures for the higher value of density, consistent with previous calculations where higher density implies more optical pumping, higher plasma ionization, more Al XIII emission relative to Al XII emission at a given temperature, and, consequently, a lower temperature determination for the same line ratio value. Interestingly enough, this pattern is broken for the two line ratios involving the satellite lines, which predict lower temperatures at the lower density. The essential difference in this case is that the satellite lines are optically thin ($\tau_0\simeq0.1$) at these temperatures and densities, whereas the resonance lines are strongly self-absorbed. At higher densities, this attenuation of resonance line photons is increased for two reasons; more absorbing centers per path length and more collisional quenching of the $2p$ levels in Al XII and Al XIII. Thus, for a given temperature, the higher the density, the larger will be the line ratio. Since the two ratios decrease with increasing temperature (at constant density), as seen in Fig. 5, this translates into lower temperature predictions as the density increases. In the 250-μm plasmas, the opacity effects were approximately a factor of 6 (1400/250) smaller, and only small deviations with density occurred in the two ratios, as seen from Fig. 5.

Summarizing the gradient effects on the temperature-sensitive line ratios, Fig. 12 illustrates why temperatures which are universally lower than the average temperature, are predicted from the laser-foil interaction spectrum. Essentially, the emission from every K-shell line, except $1s^2$-$1s2p\,{}^1P$, is heavily weighted in the high-density colder region of the plasma near 0.015 cm, where the electron temperature is about 600–650 eV. The Al XII resonance line shows no weighting in the dense regions, but, due to strong photon pumping, emits strongly over the entire plasma expanse. Since no fall off with density occurs for this line, the $L\alpha/1s^2$-$1s2p$ line ratio will display this behavior along with that of the $L\alpha$ emission, which reflects mostly the dense-plasma conditions at the emission peak. Consequently, the temperature indicated by this ratio is more a function of the plasma size than of the temperature or density gradients present.

The continuum slopes from previous calculations have also indicated temperatures which are larger than the average temperature. However, as did the lines, they underestimate the averate T_e for the laser-foil interaction. Since the plasma is optically thin to both the Al XIV and Al XIII recombination photons, the only competing effects in determining the continuum emission are the density- and power-function weighting. Since the values in Table I are much lower than the actual average T_e, the density weighting is undoubtedly the dominant factor. If the plasma temperature is emitter averaged, rather than volume averaged, such that

$$\overline{T}_e=\frac{\sum_j N_I(j)V(j)T_e(j)}{\sum_j N_I(j)V(j)}\,, \tag{2}$$

where $N_I(j)$ and $V(j)$ are the ion density and volume in zone j, not surprisingly, the value obtained, 340 eV, is not far from the average of the two continuum temperatures. However, the fact that the electron temperature is about 800 eV over 90% of the K-shell emitting region is *not* reflected in either line or continuum measurements if the isothermal, isodense plasma assumption is used in the analysis.

IV. DISCUSSION

To summarize this investigation, a one-dimensional CRE plasma ionization-radiation model was used to investigate the effect of density and temperature gradients on commonly used plasma spectral diagnostics. The theoretical spectra from several density and temperature profiles were analyzed using data calculated by the model assuming the plasma to be isothermal and isodense, and the results compared to the actual temperatures and densities used to generate these spectra.

Ion densities determined from two density-sensitive line intensity ratios displayed differences on the order of 25–50% based on uncertainties in the electron temperature of about a factor of 2. This seems quite reasonable, since uncertainties of 50% in density are usually acceptable for this plasma parameter. In fact, the intercombination-to-resonance line ratio alone is probably a suffi-

cient density indicator at these densities. At higher densities, the $1s2p\ ^3P$-$2p^2\ ^3P/1s2s\ ^3S$-$2s2p\ ^3P$ line ratio can lend even greater confidence to the analysis. At very high densities, these lines become broadened and overlap, complicating the density measurement; in this case, different ratios need to be investigated or Stark widths must be used to obtain accurate values for the plasma density.

Electron temperature measurements, based on line intensity ratios, varied over a wide range for the plasmas studied, usually about 200–300 eV. In addition, the value obtained by averaging these measurements was usually quite different from the actual volume-averaged temperature. Studies showed that this was due to the following three effects:

(1) Optical pumping of Al XII and Al XIII excited states preferentially enchanced certain emission lines, biasing the temperature measurement up or down depending on whether the Al XIII or Al XII lines were more optically thick. Thus, the temperature measurement is dependent on the *direction* of the temperature gradient.

(2) The K-shell lines exhibit a power density which varies with T_e in a way that displays a clear maximum. The existence of this maximum weights the line emission in the region where the plasma is at a temperature at or near the temperature corresponding to this peak in the power density. Since the line emission is more intense in this region, the line ratio will be appropriately weighted there also. Moreover, if the two lines comprising the ratio peak at different temperatures, the two line emissions will be weighted in *different* regions.

(3) The ion density distribution affects the emission characteristics. Since more emitters exist in regions of higher density, the line emission (and thus, the temperature measurement) will be biased in favor of these regions. Although a density gradient in an isothermal plasma was shown to cause little change in the temperature determination, it is the *combined* effect of density and temperature gradients which causes the large discrepancies between actual and measured temperature values.

If the density weighting is the dominating effect of the three factors, the reduced electron temperature may be somewhat representative of the *mass-averaged* temperature. However, it is difficult to determine this fact *a priori* when analyzing a spectrum.

The slopes of the Al XIII and Al XII recombination continua appeared to predict more accurate average temperatures than the line ratios, particularly if the two values are averaged. This is perhaps due to the fact that the plasma was optically thin to these continuum photons, biasing the measurements by only the factors (2) and (3) above. Nevertheless, they do not constitute a reliable temperature diagnostic free of the effects of the plasma gradients.

A trend was noted in the case of the j-k satellite-to-resonance line ratio. The temperature deduced from this ratio was consistently lower (or higher, depending on the direction of the gradients) than those predicted by other ratios. Apparently, this phenomenon is a clear indicator of the existence of temperature gradients in the K-shell emitting region of the plasma. In comparisons of theory with experiment, it is often the case that we have reasonably fit every line in the K spectrum except the j-k satellite line.[8] In view of this study, the reason for this commonly occurring discrepancy is now evident.

What conclusions can be drawn from this analysis? Essentially, it is naive to rely on a single temperature diagnostic when analyzing K-shell spectra from laboratory plasmas in the range of densities studied here. In fact, this statement may be true for many plasmas at much lower densities, where the power-density function alone can affect the temperature determination when gradients are present. The alternative is to use every possible feature of the K spectrum in the analysis. Good agreement on *all* of the more prominent features of the spectrum would be a rather convincing argument for accurate modeling. This could be quite arduous, however, since there are many combinations of density and temperature gradients to choose from in attempting to generate a theoretical spectrum which compares one to one with experiment. Of course, this task can be facilitated greatly if the *absolute* line intensities are known. Instead of using line ratios for parameter determinations, each individual line now becomes a useful diagnostic.

The ultimate solution, however, may be the complete modeling of the dynamic plasma, combining MHD calculations with detailed ionization and radiation transport models. In the past, this has proved to be too time consuming on existing computers. However, using the radiation model in this calculation based on photon probability of escape, the combined calculations are not prohibitively expensive, and self-consistent calculations can (and are currently) being done. In particular, we have found that by retaining only a few energetically important (K- and L^7-shell) lines in our radiation-hydrodynamic model, temperature and density profiles throughout the plasma time evolution can be postprocessed with more complete radiation

models, either the one described here or a frequency-by-frequency ray-trace transport scheme.[21] In this way, a detailed record of the plasma radiation signature is obtainable along with the self-consistent modeling of the dynamic plasma.

ACKNOWLEDGMENTS

The authors would like to thank H. R. Griem for helpful discussions and suggestions regarding the manuscript. This research was supported by the Defense Nuclear Agency.

[1]H. R. Griem, *Plasma Spectroscopy* (McGraw-Hill, New York, 1964).
[2]A. V. Vinogradov, I. Yu. Skobelev, and E. A. Yukov, Zh. Eksp. Teor. Fiz. 72, 1762 (1977) [Sov. Phys.—JETP 45, 925 (1977)].
[3]T. Holstein, Phys. Rev. 72, 1212 (1947); 83, 1159 (1951).
[4]F. E. Irons, J. Quant. Spectrosc. Radiat. Transfer 22, 1 (1979) and references contained therein.
[5]D. Duston and J. Davis, Phys. Rev. A 21, 932 (1980).
[6]D. Duston and J. Davis, Phys. Rev. A 21, 1664 (1980).
[7]D. Duston and J. Davis, Phys. Rev. A 23, 2602 (1981).
[8]D. Duston and J. Davis, J. Quant. Spectrosc. Radiat. Transfer (in press).
[9]P. G. Burkhalter, D. Duston, J. Davis, J. E. Rauch, and M. Gersten, Bull. Am. Phys. Soc. 25, 690 (1980).
[10]D. R. Bates, A. E. Kingston, and R. W. P. McWhirter, Proc. R. Soc. London Ser. A 267, 297 (1962).
[11]J. P. Apruzese, J. Davis, D. Duston, and K. G. Whitney, J. Quant. Spectrosc. Radiat. Transfer 23, 479 (1980).
[12]A. Burgess, H. P. Summers, D. M. Cochrane, and R. W. P. McWhirter, Mon. Not. R. Astron. Soc. 179, 275 (1977).
[13]A. K. Pradhan, D. W. Norcross, and D. G. Hummer, Phys. Rev. A 23, 619 (1981); Astrophys. J. 246, 1031 (1981).
[14]K. G. Whitney and J. Davis, J. Appl. Phys. 45, 5294 (1974).
[15]J. C. Weisheit, C. B. Tarter, J. H. Scofield, and L. M. Richards, J. Quant. Spectrosc. Radiat. Transfer 16, 659 (1976).
[16]R. K. Landshoff and J. D. Perez, Phys. Rev. A 13, 1619 (1976).
[17]A. L. Hoffman and E. A. Crawford, J. Appl. Phys. 49, 3219 (1978).
[18]D. Salzmann and A. Krumbein, J. Appl. Phys. 49, 3229 (1978).
[19]D. Duston and J. J. Duderstadt, Phys. Rev. A 18, 1707 (1978).
[20]H. Yasuda and T. Sekiguchi, Jpn. J. Appl. Phys. 18, 2245 (1979).
[21]K. G. Whitney, J. Davis, and J. P. Apruzese, Phys. Rev. A 22, 2196 (1980).
[22]A. H. Gabriel, Mon. Not. R. Astron. Soc. 160, 99 (1972).
[23]A. H. Gabriel and T. M. Paget, J. Phys. B 5, 673 (1972).
[24]C. P. Bhalla, A. H. Gabriel, and L. P. Presnyakov, Mon. Not. R. Astron. Soc. 172, 359 (1975).
[25]J. C. Weisheit, J. Phys. B 8, 2556 (1975).
[26]L. P. Presnyakov, Usp. Fiz. Nauk 119, 49 (1976) [Sov. Phys.—Usp. 19, 387 (1976)] and references contained therein.
[27]V. L. Jacobs and M. Blaha, Phys. Rev. A 21, 525 (1980).
[28]H.-J. Kunze, A. H. Gabriel, and H. R. Griem, Phys. Fluids 11, 662 (1968).
[29]E. V. Aglitskii, V. A. Boiko, A. V. Vinogradov, and E. A. Yukov, Kvant. Elektron. (Moscow) 1, 579 (1974) [Sov. J. Quantum Electron. 4, 322 (1974)].
[30]A. V. Vinogradov, I. Yu. Skobelev, and E. A. Yukov, Kvant. Elektron. (Moscow) 2, 1165 (1975) [Sov. J. Quantum Electron. 5, 630 (1975)].
[31]V. A. Boiko, A. Ya. Faenov, S. A. Pikuz, I. Yu. Skobelev, A. V. Vinogradov, and E. A. Yukov, J. Phys. B 10, 3387 (1977).
[32]I. Yu. Skobelev, A. V. Vinogradov, and E. A. Yukov, Phys. Scr. 18, 78 (1978).
[33]S. Goldsmith, J. Phys. B 2, 1075 (1969).
[34]A. V. Vinogradov, I. Yu. Skobelev, and E. A. Yukov, Zh. Eksp. Teor. Fiz. 72, 1762 (1977) [Sov. Phys.—JETP 45, 925 (1977)].
[35]J. F. Seely, Phys. Rev. Lett. 42, 1606 (1979).
[36]J. Davis, NRL Memorandum Report No. 2655, 1973 (unpublished).
[37]C. M. Lee and A. Hauer, Appl. Phys. Lett. 33, 692 (1978).
[38]J. Davis and M. Blaha, J. Quant. Spectrosc. Radiat. Transfer (in press).
[39]I. L. Beĭgman, V. A. Boĭko, S. A. Pikuz, and A. Ya. Faenov, Zh. Eksp. Teor. Fiz. 71, 975 (1976) [Sov. Phys.—JETP 44, 511 (1976)].
[40]F. E. Irons, J. Quant. Spectrosc. Radiat. Transfer 24, 119 (1980).
[41]B. Yaakobi *et al.*, Phys. Rev. A 19, 1247 (1979).
[42]J. D. Kilkenny, R. W. Lee, M. H. Key, and J. G. Lunney, Phys. Rev. A 22, 2746 (1980).
[43]A. Hauer *et al.*, Phys. Rev. Lett. 45, 1495 (1980).
[44]V. L. Jacobs and J. Davis, NRL Memorandum Report No. 4365 (unpublished).
[45]N. J. Peacock, M. G. Hobby, and M. Galanti, J. Phys. B 6, L298 (1973).
[46]U. Feldman *et al.*, Astrophys. J. 192, 213 (1974).
[47]M. Bitter *et al.*, Phys. Rev. Lett. 43, 129 (1979).
[48]R. U. Datla, L. A. Jones, and D. B. Thomson, Los Alamos Report No. LA-8324-MS (unpublished).
[49]C. Stallings, K. Nielsen, and R. Schneider, Appl. Phys. Lett. 29, 404 (1976).
[50]P. Burkhalter *et al.*, J. Appl. Phys. 50, 705 (1979).
[51]E. L. Kane, D. Duston, and J. Davis, Bull. Am. Phys. Soc. 25, 849 (1980).
[52]E. A. McLean *et al.*, Phys. Rev. Lett. 45, 1246 (1980).
[53]D. G. Colombant, K. G. Whitney, D. A. Tidman, N. K. Winsor, and J. Davis, Phys. Fluids 18, 1687 (1975).
[54]R. W. Clark, J. Davis, and D. Duston, Bull. Am. Phys. Soc. 25, 1014 (1980).